The molecular pathogenesis of the *NUP98-HOXA9* fusion protein in Acute Myeloid Leukemia

Ana Rio-Machin [1,2]; Gonzalo Gomez-Lopez [3]; Javier Muñoz [4]; Fernando Garcia-Martinez [4]; Alba Maiques-Diaz [1]; Sara Alvarez [1]; Rocio N Salgado [1]; Mahesh Shrestha [5]; Raúl Torres [6]; Claudia Haferlach [7]; Maria Jose Larrayoz [8]; Maria Jose Calasanz [8]; Jude Fitzgibbon [2] and Juan C. Cigudosa [1]

[1] Molecular Cytogenetics Group, Human Cancer Genetics Programme, Centro Nacional Investigaciones Oncologicas (CNIO), Madrid, Spain

[2] Centre for Haemato-Oncology, Barts Cancer Institute, Queen Mary University of London, UK

[3] Bioinformatics Unit, Centro Nacional Investigaciones Oncologicas (CNIO), Madrid, Spain

[4] Proteomics Unit, Centro Nacional Investigaciones Oncologicas (CNIO), Madrid, Spain. ProteoRed-ISCIII.

[5] Division of Experimental Hematology and Cancer Biology, Cincinnati Children's Hospital Medical Center, Cincinnati, OH, USA

[6] Viral Vector Facility, Fundacion Centro Nacional de Investigaciones Cardiovasculares (CNIC), Madrid, Spain

[7] MLL Münchner Leukämielabor, München, Germany

[8] Department of Genetics and Center for Applied Medical Research (CIMA), University of Navarra, Pamplona, Spain

Corresponding author:

Ana Rio-Machin, PhD
Centre for Haemato-Oncology
Barts Cancer Institute
Queen Mary University of London
John Vane Science Centre, Charterhouse Square,
London EC1M 6BQ (United Kingdom)
Tel: +44 (0)20 7882 8780
Email: a.rio-machin@qmul.ac.uk

DISCLOSURE OF CONFLICTS OF INTEREST

The authors have declared that no conflict of interest exists.

Recurrent chromosomal translocations are common initiation events and have provided important insights into the pathogenesis of AML, paving the way for the introduction of novel targeted therapies. However, clinical outcomes, in particular for patients with adverse cytogenetic features remain suboptimal. The chromosomal translocation t(7;11)(p15, p15), encoding the fusion protein NUP98-HOXA9 (NHA9), is a rare poor risk cytogenetic event in AML associated with a particularly poor prognosis. NHA9 brings the FG repeat-rich portion of the nucleoporin NUP98 upstream of the homeodomain and *PBX* heterodimerization domains of HOXA9, and acts as oncogenic transcription factor [1]. The pathogenic events underlying NHA9 remain poorly understood and herein, we aim to characterize the downstream mediators of this oncoprotein by determining the effects of the fusion using human cellular models.

We set out initially to compare the DNA binding sites of *NHA9*, *HOXA9* and *NUP98*, by forced expression of these genes alone or the corresponding fusion gene by retroviral transduction of HEK93FT cell line and cord blood-isolated human hematopoietic progenitors (hHP). ChIP-seq analysis in the HEK293FT cellular model identified 4 471 significant genomic regions (false discovery rate (FDR) < 0.05) as target sites of the fusion protein, all located within -5/+ kb from the annotated Transcription Start Site (TSS) (Figure S1A). They correspond to 1 368 genes and 17 miRNAs (Table S1) of which 399 genes were also shown to be common targets of *HOXA9* and 4 of *NUP98* (Figure 1A, Table S2, Figures S1C-D) [See supplementary methods] (Data deposited in GEO http://www.ncbi.nlm.nih.gov/geo/, accession number: GSE62587). Ingenuity pathway analysis of the NHA9 target series demonstrated a significant enrichment of pathways associated with tumorigenesis and leukemic differentiation (Figure S1B).

We next performed a detailed sequence analysis of the NHA9 binding sites using the MEME-ChIP algorithm and detected a significant overlap with binding of several HOX genes, including *HOXA9*, supporting a role for this homeodomain in the DNA binding of NHA9. Strikingly, NHA9 sites were enriched for a novel binding motif, CA/gTTT, that was present in one-third (n = 1 421) of all NHA9 ChIP-seq regions (Table S3). This motif had not been previously associated with any known transcription

factor and was not observed in wild type *HOXA9* or *NUP98* binding site experiments, suggesting that it is specific to NHA9 DNA binding. MEME-ChIP (SpaMO) was used to identify significant co-occurrences of other known DNA binding motifs with this novel NHA9 DNA binding motif. Binding motifs corresponding to 12 transcription factors, including other HOX family proteins such as HOXB7 or HOXD11, were found to be overrepresented within the region adjacent to CA/gTTT (Table S4), suggesting a possible functional cooperation with the fusion oncoprotein.

As the NHA9 target motifs are preferentially located more than 1 kb upstream/downstream of the TSS (Figure S1A), we reasoned that NHA9 binding may coincide with particular enhancer elements. A similar distribution was also found for the identified *HOXA9* target regions whereas *NUP98* binding sites were mostly located within promoters, both in agreement with previous studies [2, 3]. We selected eight leukemia-related genes (*MEIS1, HOXA9, PBX3, MET, BRAF, AF9, PTEN* and *NF1)* identified as part of our NHA9 ChIP-seq experiments, for locus specific qChIP studies. A significant enrichment of H3K4me1, a chromatin mark that predicts poised and active enhancers, and RNA Polymerase II (PolII), which is consistent with the presence of the active form of the enhancers [4, 5], was shown within the NHA9 binding sites upstream of the eight genes (Figures 1B and S1E). NHA9 expression levels were demonstrated to be comparable in our two cellular models (HEK293FT and hHP) (Figure S1G). Accordingly, we validated the ChIP-seq results in the HEK293FT model (Figure S1F) using the same set of eight NHA9 target genes and also demonstrated binding of NHA9 to the eight enhancers in our second model system of NHA9-expressing hHP cells (Figure 1C), allowing us to confirm these findings in primary human hematopoiesis.

We next focused attention on the transcription factors *MEIS1, HOXA9* and *PBX3*, as their overexpression is significantly related to adverse prognosis in AML (The Cancer Genome Atlas [6]; Figure S1H) and were previously reported to drive leukemogenesis through the formation of a transcriptional activator complex [7]. To test the importance of these three transcription factors in NHA9 pathogenesis, we completed reporter assays in HEK293FT cells by cloning the identified enhancers of *MEIS1, HOXA9* or *PBX3* into a luciferase reporter vector. A significant 1.6-2.8 fold induction in luciferase activity was

observed when NHA9 was co-expressed for all three enhancers, indicating a direct induction of *MEIS1, HOXA9* and *PBX3* expression through the NHA9 interaction with their corresponding regulatory regions (Figure 1D) [see Supplementary Methods]. This observation was accompanied by upregulation of all 3 transcription factors and of three of their known target genes (*MYB, MEF2C* and *FLT3*) [7] in NHA9-expressing hHP cells (Figure 1E and S1I). Gene Expression Profiling performed in three independent NHA9-expressing hHP clones and AMLs from 5 patients with t(7;11)(p15,p15), confirmed *MEIS1-HOXA9-PBX3* overexpression and it was further validated by RT-qPCR analysis in 3 additional NHA9 primary samples (Figure S2A). These observations suggested that the NHA9-expressing hHP cells can be sensitive to HXR9, a specific peptide inhibitor of HOXA9 and PBX3 interaction that leads to disruption of the MEIS1-HOXA9-PBX3[8] complex. We tested this hypothesis by treating these cells with HXR9 that resulted in a selective decrease in their viability (Figure 1F and S2B-D) [see Supplementary Methods] without affecting cell differentiation (data not shown), therefore confirming the relevance of these downstream mediators in driving the oncogenic activity of NHA9.

In order to explore other mechanisms driving NHA9 pathogenesis and to better understand its role in transcriptional regulation, we interrogated our ChIP-seq and gene expression profiling data, which revealed both activation and repression of gene expression induced by this fusion oncoprotein (Figure 2A). The cooperation of MLL1 and CRM1 with NHA9 in the upregulation of some target genes has been shown recently by Xu *et al*. [9, 10], which was also supported by comparing NHA9 target genes identified in our ChIP-seq experiments with MLL1 and CRM1 targets. We found that 25% and 35% of NHA9 target genes were also in common with MLL1 and CRM1 target genes, respectively (Figure S2E). Notably, 151 target genes, including *MEIS1* and *HOXA9*, were shared by all three proteins (NHA9, MLL1 and CRM1), suggesting a possible cooperation among these transcription factors in NHA9-driven leukemias. It has also been reported that NUP98, through its FG repeat domain, may interact with transcriptional activator p300 and repressor HDACs [11], allowing us to postulate that transcriptional effects of NHA9 in enhancers could be mediated by these regulators. We first demonstrated NHA9 binding to both p300 and HDAC1 by Co-immunoprecipitation experiments (Figure 2B) [see

Supplementary Methods] and went on to examine their binding potential in a panel of eight regulatory regions of NHA9 target genes (four upregulated and four downregulated target genes) in the presence of the fusion protein by qChIP. These experiments demonstrated selective binding of p300 to the regulatory regions of the upregulated genes *MEIS1, HOXA9, PBX3* and *AFF3* (Figure 2C), and of HDAC1 to the downregulated genes *BIRC3, SMAD1*, *FILIP1L* and *PTEN* (Figure 2D). Altogether this data suggests that p300 and HDAC1 are selectively recruited by NHA9 at enhancer regions to modulate the expression of genes involved in leukemogenesis.

As the interaction of NHA9 with HDAC1/2 was validated by mass spectrometry analysis using the NHA9-expressing HEK293FT model (Proteomics data have been deposited on the ProteomeXchange Consortium via the PRIDE partner repository, data set identifier PXD001828)) [see Supplementary Methods], we had a molecular rationale for testing HDAC inhibitors (HDACi) in NHA9 AML. We assessed the sensitivity of the hHP-NHA9 model to the pan-HDACi LBH589 (Panobinostat) and observed a strong inhibitory effect that was significantly higher ($IC50_{hHP\text{-}NHA9}$≈4nM) than its inhibitory effect in MLL-AF9 -expressing ($IC50_{hHP\text{-}MLL\_AF9}$≈30nM) or AML1-ETO-expressing ($IC50_{hHP\text{-}AML1\_ETO}$≈200nM) hHP cells [12, 13], where the efficacy of this component has been already established [14, 15] (Figure 2E). Accordingly, treatment with low doses (4nM) of LBH589 completely abrogated the ability of hHP-NHA9 cells to form colonies in the CFC assay (Figure S2F) and significantly induced apoptosis within 24h (4nM and 30nM doses), whereas LBH589 had no effect at the same doses on the empty vector control hHP cells (Figure S2G). It has to be noted that LBH589 did not induce differentiation in NHA9-expressing cells as no significant changes in the number of CD11b positive cells were observed by flow cytometry analysis post treatment (data not shown). These observations are in accordance with a recent report suggesting the combination of COX or DNMT inhibitors with HDACi for treatment of NHA9 AML patients [16], however in this study we identified the molecular rationale for HDACi therapy as well as a panel of target genes downstream of NHA9 that can be used as biomarkers for response to this treatment. Furthermore, our hHP-NH9A cellular model showed sensitivity to markedly lower concentrations of LBH589 (4nM) than the recommended doses in

preclinical studies and Multiple Myeloma Clinical Trials [17, 18], indicating that LBH589 could be safely used as novel targeted therapy for the treatment of NH9A AML patients. However, the biological consequences of this therapy, as well as the best dosage-time relation for the translation into clinics need to be further investigated.

In summary, NHA9 deregulates the expression of key leukemic genes, including *MEIS1-HOXA9-PBX3* complex, through the enhancer binding and the direct interaction of the fusion protein with HDAC and p300 transcriptional regulators. The oncogenic effects of NHA9 can be overcome by HDACi treatment, demonstrating a significant inhibitory effects against NHA9-driven leukemic cells and suggesting a novel approach to treatment of this high-risk group of patients.

Supplementary information is available at Leukemia's website

(http://www.nature.com/leu/index.html)

REFERENCES

1. Takeda A, Goolsby C, Yaseen NR. NUP98-HOXA9 induces long-term proliferation and blocks differentiation of primary human CD34+ hematopoietic cells. *Cancer research* 2006 Jul 1; **66**(13)**:** 6628-6637.

2. Huang Y, Sitwala K, Bronstein J, Sanders D, Dandekar M, Collins C*, et al.* Identification and characterization of Hoxa9 binding sites in hematopoietic cells. *Blood* 2012 Jan 12; **119**(2)**:** 388-398.

3. Liang Y, Franks TM, Marchetto MC, Gage FH, Hetzer MW. Dynamic association of NUP98 with the human genome. *PLoS genetics* 2013; **9**(2)**:** e1003308.

4. Smith E, Shilatifard A. Enhancer biology and enhanceropathies. *Nature structural & molecular biology* 2014 Mar; **21**(3)**:** 210-219.

5. De Santa F, Barozzi I, Mietton F, Ghisletti S, Polletti S, Tusi BK*, et al.* A large fraction of extragenic RNA pol II transcription sites overlap enhancers. *PLoS biology* 2010 May; **8**(5)**:** e1000384.

6. Cancer Genome Atlas Research N. Genomic and epigenomic landscapes of adult de novo acute myeloid leukemia. *The New England journal of medicine* 2013 May 30; **368**(22)**:** 2059-2074.

7. Garcia-Cuellar MP, Steger J, Fuller E, Hetzner K, Slany RK. Pbx3 and Meis1 cooperate through multiple mechanisms to support Hox-induced murine leukemia. *Haematologica* 2015 Jul; **100**(7)**:** 905-913.

8. Li Z, Zhang Z, Li Y, Arnovitz S, Chen P, Huang H*, et al.* PBX3 is an important cofactor of HOXA9 in leukemogenesis. *Blood* 2013 Feb 21; **121**(8)**:** 1422-1431.

9. Xu H, Valerio DG, Eisold ME, Sinha A, Koche RP, Hu W*, et al.* NUP98 Fusion Proteins Interact with the NSL and MLL1 Complexes to Drive Leukemogenesis. *Cancer cell* 2016 Dec 12; **30**(6)**:** 863-878.

10. Oka M, Mura S, Yamada K, Sangel P, Hirata S, Maehara K*, et al.* Chromatin-prebound Crm1 recruits Nup98-HoxA9 fusion to induce aberrant expression of Hox cluster genes. *eLife* 2016 Jan 07; **5:** e09540.

11. Moore MA, Chung KY, Plasilova M, Schuringa JJ, Shieh JH, Zhou P*, et al.* NUP98 dysregulation in myeloid leukemogenesis. *Annals of the New York Academy of Sciences* 2007 Jun; **1106:** 114-142.

12. Wei J, Wunderlich M, Fox C, Alvarez S, Cigudosa JC, Wilhelm JS*, et al.* Microenvironment determines lineage fate in a human model of MLL-AF9 leukemia. *Cancer cell* 2008 Jun; **13**(6)**:** 483-495.

13. Mulloy JC, Cammenga J, Berguido FJ, Wu K, Zhou P, Comenzo RL*, et al.* Maintaining the self-renewal and differentiation potential of human CD34+ hematopoietic cells using a single genetic element. *Blood* 2003 Dec 15; **102**(13)**:** 4369-4376.

14. Bots M, Verbrugge I, Martin BP, Salmon JM, Ghisi M, Baker A*, et al.* Differentiation therapy for the treatment of t(8;21) acute myeloid leukemia using histone deacetylase inhibitors. *Blood* 2014 Feb 27; **123**(9)**:** 1341-1352.

15. Baker A, Gregory GP, Verbrugge I, Kats L, Hilton JJ, Vidacs E*, et al.* The CDK9 Inhibitor Dinaciclib Exerts Potent Apoptotic and Antitumor Effects in Preclinical Models of MLL-Rearranged Acute Myeloid Leukemia. *Cancer research* 2016 Mar 1; **76**(5)**:** 1158-1169.

16. Deveau AP, Forrester AM, Coombs AJ, Wagner GS, Grabher C, Chute IC*, et al.* Epigenetic therapy restores normal hematopoiesis in a zebrafish model of NUP98-HOXA9-induced myeloid disease. *Leukemia* 2015 Oct; **29**(10)**:** 2086-2097.

17. Anne M, Sammartino D, Barginear MF, Budman D. Profile of panobinostat and its potential for treatment in solid tumors: an update. *OncoTargets and therapy* 2013; **6:** 1613-1624.

18. San-Miguel JF, Hungria VT, Yoon SS, Beksac M, Dimopoulos MA, Elghandour A*, et al.* Panobinostat plus bortezomib and dexamethasone versus placebo plus bortezomib and dexamethasone in patients with relapsed or relapsed and refractory multiple myeloma: a multicentre, randomised, double-blind phase 3 trial. *The Lancet Oncology* 2014 Oct; **15**(11)**:** 1195-1206.

FIGURE 1

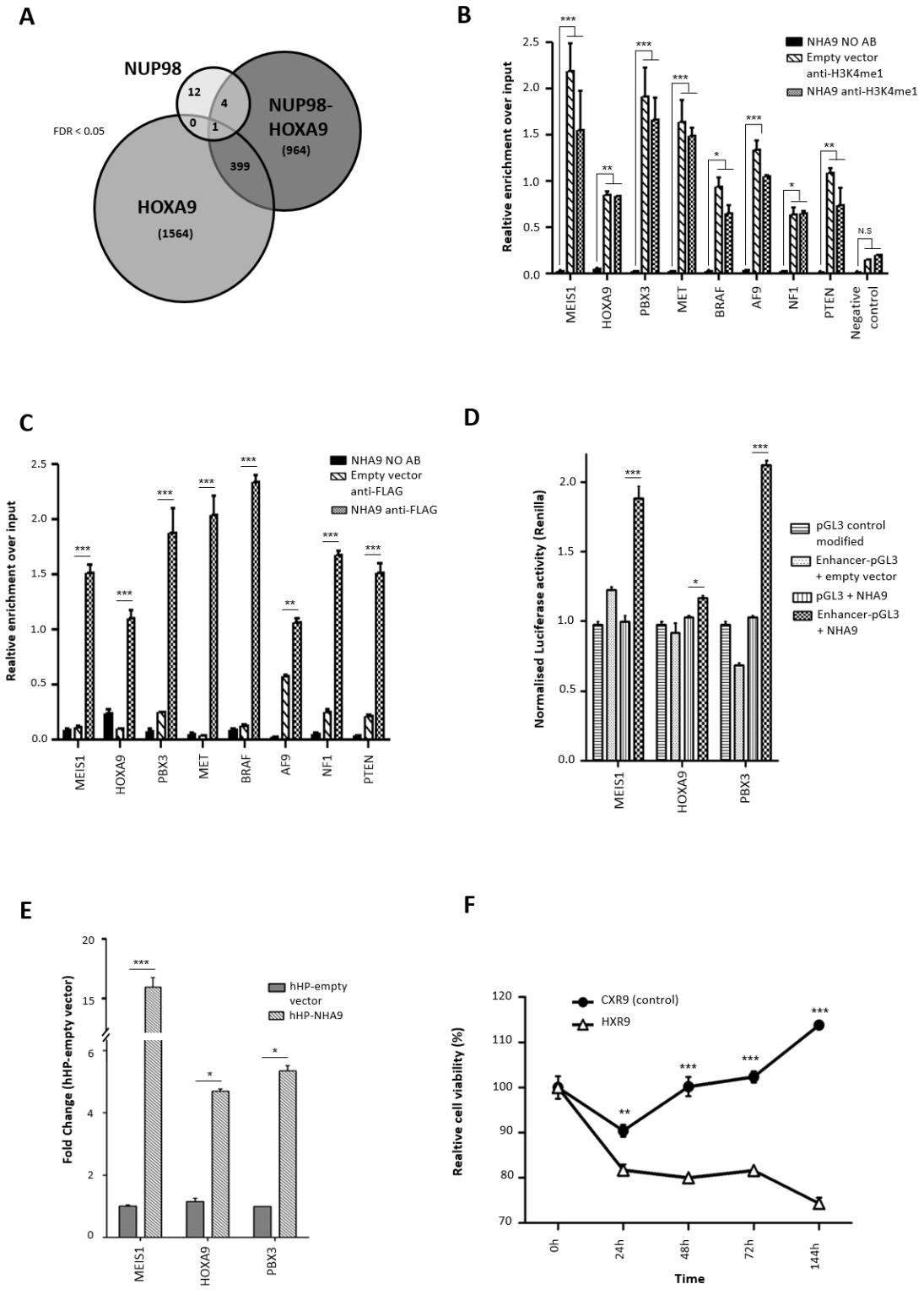

Figure 1: NUP98-HOXA9 binds to enhancers of genes related to leukemogenesis (A) Venn diagrams of NHA9, HOXA9 and NUP98 target genes identified by ChIP-seq experiments on HEK293FT human models and located within +5/-5 kb of an annotated Transcrption Start Site (TSS). Significant ChIP-seq

peaks were established at FDR ≤ 5%. **(B)** H3K4me1 qChIP fold enrichment in the selected NHA9 target regions using anti-H3K4me1 antibody. The MEIS1 promoter region was used as a negative control. The average of three experiments is shown. Error bars represent SEM. **(C)** NHA9 qChIP fold enrichment on the eight selected NHA9 target enhancer regions using *anti-FLAG* antibody in the NHA9 expressing hHP cellular model. The average of 3 experiments is shown. Error bars represent SEM. **(D)** Luciferase assay was performed to analyze the role of NHA9 in regulating the expression of *HOXA9, PBX3* and *MEIS1*. The luciferase constructs containing the enhancer region (using *pGL3-Promoter* vector, Promega Biotech Ibérica S.L) of *HOXA9, PBX3* and *MEIS1* were co-transfected into HEK293FT cells with the expression vector pMSCV-NHA9, together with Renilla vector for the purpose of normalization. Luciferase activity was determined 48 h after reporter plasmid transfection in all cases. A significant increase in luciferase activity induced by NHA9 expression was observed in each case, confirming a direct increase of *MEIS1, HOXA9* and *PBX3* expression through NHA9 interaction with their corresponding enhancer regions. Data are presented as the mean value from two separate experiments with n=3 for each experiment. Error bars represent SEM. **(E)** Expression analysis by qRT-PCR of *MEIS1, HOXA9* and *PBX3* in the NHA9 expressing hHP cellular model. The expression of the endogenous human housekeeping gene GAPDH was used to normalize the data, which are expressed as the mean of $2^{-\Delta Ct}$ values obtained for each sample after normalization based on the hHP-empty vector model. **(F)** Analysis of the hHP-NHA9 response to HXR9 and *CXR9* (control) peptides. hHP-NHA9 cells were plated in 96-well plates in triplicate and exposed to 13uM of HXR9/CXR9. Cell viability was assessed at different time points. Average normalized optical density (OD) values of three independent experiments are shown.

Statistical significance for relative enrichment and proliferation was determined at $p < 0.05$ (*), $p < 0.01$ (**) and $p < 0.001$ (***), using a t-test with Bonferroni correction. N.S corresponds to non-significant comparisons. Error bars represent SEM.

FIGURE 2

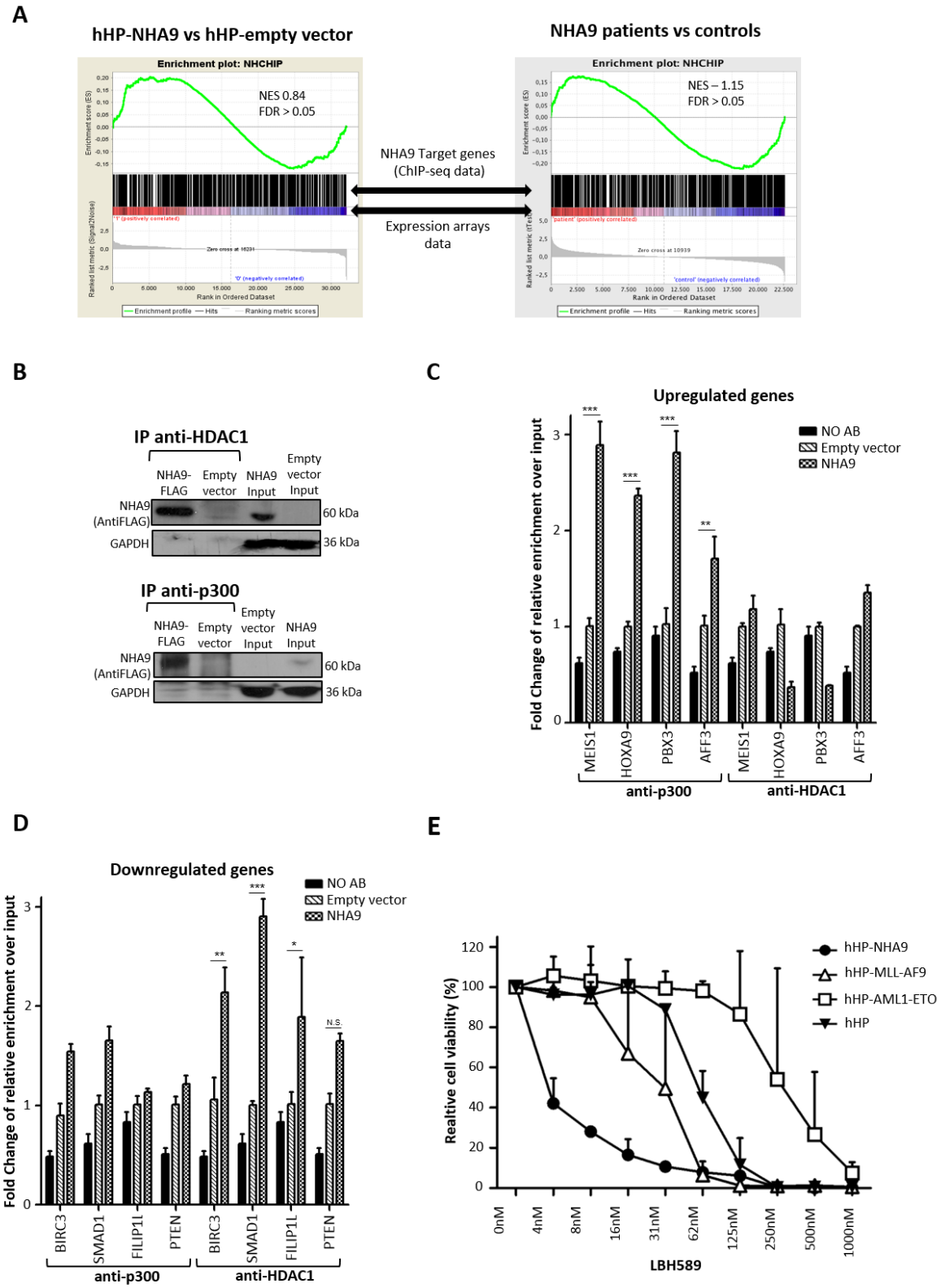

Figure 2: NUP98-HOXA9 has an activator-repressor role in transcriptional regulation driven by *p300* and *HDAC1* interactions. (A) We applied gene set enrichment analysis (GSEA) to test for enrichment

of NHA9 ChIP-seq target gene set among differentially expressed genes using expression array data from hHP-NHA9 cellular model (left panel) and five NHA9 primary samples (right panel). Genes were ranked based on the limma-moderated t statistic. After Kolmogorov-Smirnoff testing, those gene sets with FDR <0.25, a well-established cut-off for the identification of biologically relevant gene sets, were considered enriched **(B)** Analysis of NHA9 and p300/HDAC1 interactions by co-immunoprecipitation. HEK293FT cells were transfected with pMSCV-NUP98-HOXA9 or pMSCV-empty vectors. 48h post-transfection, the immunoprecitpitation was performed using *anti-p300* and *anti-HDAC1* antibodies and the proteins were analyze by immunoblotting using *anti-FLAG* antibody. Endogenous *GAPDH* protein levels were used as a loading control. **(C & D)** qChIP fold enrichment of p300 and HDAC1 in the regulatory regions of four upregulated (C) and four downregulated (D) target genes of NHA9. The average of 3 experiments showed the binding, along with the fusion protein, of p300 and HDAC1 to the regulatory regions of the overexpressed and downregulated NHA9-target genes, respectively. **(E)** Analysis of the hHP-NHA9 response to HDAC inhibitors. Cells were exposed for 72 hours to serial dilutions of panobinostat (LBH589) followed by the addition of WST-1 to assess cell viability. The average normalized optical density (OD) values are shown compared to vehicle.

Statistical significance for relative enrichment and proliferation was determined at $p < 0.05$ (*), $p < 0.01$ (**) and $p < 0.001$ (***), using a t-test with Bonferroni correction. N.S corresponds to non-significant comparisons. Error bars represent SEM.